MOLECULAR AND CELLULAR BIOLOGY, June 2006, p. 4327–4338 Vol. 26, No. 11
0270-7306/06/$08.00+0 doi:10.1128/MCB.02393-05

Phosphorylation of Amyloid Precursor Protein (APP) at Thr668 Regulates the Nuclear Translocation of the APP Intracellular Domain and Induces Neurodegeneration

Keun-A Chang,[1] Hye-Sun Kim,[1] Tae-Young Ha,[1] Ji-Won Ha,[1] Ki Young Shin,[1] Yun Ha Jeong,[1] Jean-Pyo Lee,[3] Cheol-Hyoung Park,[1] Seonghan Kim,[1] Tae-Kyoung Baik,[2] and Yoo-Hun Suh[1]*

Department of Pharmacology, College of Medicine, National Creative Research Initiative Center for Alzheimer's Dementia and Neuroscience Research Institute, MRC, Seoul National University, Seoul 110-799, South Korea[1]; Department of Anatomy, College of Medicine, Eulji University, Daejeon 301-832, South Korea[2]; and Department of Pediatrics, School of Medicine, University of California at San Diego, La Jolla, California[3]

Received 15 December 2005/Returned for modification 17 January 2006/Accepted 8 March 2006

Amyloid precursor protein (APP) has eight potential phosphorylation sites in its cytoplasmic domain. Recently, it has demonstrated that the constitutive phosphorylation of APP at T668 (APP695 isoform numbering) was observed specifically in the brain. Neuron-specific phosphorylation of APP at T668 is thought to be important for neuronal functions of APP, although its exact physiological significance remains to be clarified. In this study, we show that the phosphorylation of the APP intracellular domain (AICD) at T668 is essential for its binding to Fe65 and its nuclear translocation and affects the resultant neurotoxicity, possibly mediated through the induction of glycogen synthase kinase 3β and tau phosphorylation by enhancing the formation of a ternary complex with Fe65 and CP2 transcription factor. Taken together, these results suggest that the phosphorylation of AICD at T668 contributes to the neuronal degeneration in Alzheimer's disease (AD) by regulating its translocation into the nucleus and then affects neurodegeneration; therefore, the specific inhibitor of T668 phosphorylation might be the target of AD therapy.

Amyloid beta peptide (Aβ) generated from amyloid precursor protein (APP) is the main component of neuritic plaques in the brains of Alzheimer's disease (AD) patients, and its aggregation is hypothesized to be central to the pathogenesis of AD (28). APP, which is a type I transmembrane protein, is cleaved consecutively, first at the extracellular juxtamembrane region by α- or β-secretase and then at the intramembrane region by γ-secretase. Following the first cleavage, a soluble APP fragment (sAPPα or sAPPβ) is secreted, and then, following the second cleavage, p3 or Aβ peptides and the AICD (APP intracellular domain) are generated, together with release of the cytoplasmic fragment into the cytoplasm (7, 29, 31, 37, 39).

APP contains eight potential phosphorylation sites within its cytoplasmic domain (21). Seven of these potential phosphorylation sites were recently shown to be phosphorylated in AD brains, i.e., Y653, S655, T668, S675, Y682, T686, and Y687 (APP695 isoform numbering) (21). The constitutive phosphorylation of APP at T668 is observed specifically in the brain (14). The phosphorylation of APP at T668 is mediated by neuronal cyclin-dependent protein kinase 5 (cdk5) (14), p34cdc2 protein kinase (cdc2) (32), glycogen synthase kinase 3β (GSK-3β) (3), or c-jun N-terminal kinases (17, 30, 33, 34). Neuron-specific phosphorylation of APP at T668 is thought to be important for neuronal functions of APP, although its exact physiological significance remains to be clarified. T668 phosphorylation has been reported to play a role in APP metabolism by facilitating the BACE cleavage of APP to increase Aβ generation (21). However, the detailed molecular mechanism by which APP phosphorylation mediates these physiological events remains unknown.

In a multidimensional nuclear magnetic resonance study, it was shown that the phosphorylation at cytoplasmic phosphorylation sites, i.e., T654, S655, or T668, induces changes in the backbone dihedral angles of APP, which may be attributed to local hydrogen bond formation between the phosphate group and nearby amide protons. The phosphorylation of T668 results in destabilization of the amino-terminal helix capping-box structure (25) and leads to an overall conformational change in the cytoplasmic domain including the Fe65-binding motif 681-GYENPTY-687 (1). These phosphorylation-induced structural changes may act as a conformational switch in the cytoplasmic tail of APP, which may alter the binding specificity and affinity of the APP cytoplasmic tail to cytosolic partners.

APP is known to interact with several binders through functional motifs in its cytoplasmic domain (1). The phosphotyrosine interaction domains of Fe65, Fe65L1, X11, X11L, X11L2, and mammalian disabled (mDab1) interact with the ^{682}YENPTY^{687} motif of APP (5, 9, 27, 40). Additionally, PAT1, a microtubule-interacting protein, interacts with the ^{653}YTSI^{656} motif of APP and regulates its basolateral sorting (42). A recent study has shown that interaction of AICD with the adaptor protein Fe65 transactivates genes after translocating into the nucleus (8). Also, several target gene candidates that are possibly regulated by AICD-mediated and Fe65-dependent signaling have been reported (4, 15, 24, 35, 38). However, the regulation and physiological significance of AICD-mediated signaling are still largely unknown.

In this study, we aimed to elucidate the role of the phosphorylation of AICD at T668 in regulating the molecular

* Corresponding author. Mailing address: Department of Pharmacology, College of Medicine, and National Creative Research Initiative Center for Alzheimer's Dementia, Seoul National University, Seoul 110-799, South Korea. Phone: 82 2 740 8285. Fax: 82 2 745 7996. E-mail: yhsuh@plaza.snu.ac.kr.

interaction between Fe65 and AICD and the Fe65-dependent gene transactivation of AICD. Our study demonstrates that the phosphorylation of AICD at T668 is required for its translocalization to the nucleus and affects neurotoxicity by activating transcription of GSK-3β and upregulating tau phosphorylation. Moreover, we also show that inhibition of T668 phosphorylation of AICD by specific inhibitors or mutations of T668 sites dramatically reduced its nuclear translocation and the resultant neurotoxicity. In addition, we also provide in vivo evidence that neurodegeneration, phosphorylated C-terminal fragments of APP (APP-CTFs) at T668, and GSK-3β and tau phosphorylation are significantly upregulated in the serial brain sections of the human AD brains, the Tg2576 mouse brains, and AD animal model, which harbors the Swedish APP familial AD mutation gene.

MATERIALS AND METHODS

Reagents and antibodies. Roscovitine, olomoucine, indirubin-3′monoxime, 5-iodo, and iso-olomoucine were purchased from Calbiochem (Darmstadt, Germany); lithium chloride and sodium chloride were purchased from Sigma (Missouri); anti-green fluorescent protein (anti-GFP) monoclonal antibody was obtained from CLONTECH (California); anti-APP, C-terminal polyclonal antibody (C9; against the C terminus of APP) was from Chemicon (California); anti-pAPP^{T668} polyclonal antibody was from Cell Signaling (Massachusetts); anti-Flag M5 monoclonal antibody was from Sigma; anti-human phosphorylated tau (p-tau) monoclonal antibody (AT8) was from Innogenetics (Belgium); anti-GSK-3β, anti-p-GSK-3β (Tyr^{216}), and anti-tau antibodies were from Santa Cruz (California). Anti-Fe65 and anti-CP2 serum were generous gifts from J. D. Buxbaum of Mt. Sinai University and R. G. Roeder of Rockefeller University, respectively.

DNA construct and mutagenesis. The C50 construct was generated by PCR from human APP695 cDNA to encompass the last 50 amino acid residues. It was subcloned into a pcDNA3-flag vector with the flag at the N terminus, into a pEGFP-N1 vector with GFP at the carboxyl terminus, or into a pMst vector with Gal4. Mutagenesis of the YENPTY deletion or T668A mutant variants in the C50 construct was achieved using a QuikChange site-directed mutagenesis kit (Stratagene, La Jolla, California). All constructs were sequenced using an ABI310 Sequencer. Schematic diagrams of the constructs are shown in Fig. 1a.

Cell culture and transfection. PC12 cells originating from rat pheochromocytoma were plated on polyethyleneimine (0.2 mg/ml; Sigma, Missouri)-coated plates and maintained in Dulbecco's modified Eagle's medium supplemented with 10% fetal bovine serum (GIBCO BRL, New York) and 0.3% antibiotics at 37°C in 5% CO_2. PC12 cells were treated with nerve growth factor (NGF, 50 ng/ml; Calbiochem) and allowed to be differentiated for 4 days. The cerebral cortex was dissected from an embryonic day 17 Sprague-Dawley rat embryo and dissociated by gentle triturate. Cells were cultured in a specified medium for neurons (neurobasal medium supplemented with B27 and penicillin-streptomycin-amphotericin B mixture [Gibco BRL]). Experiments were performed on 14- to 15-day cultures. NGF-differentiated PC12 cells and rat cortical primary neurons were transiently transfected with individual constructs by using Fugene 6 according to the manufacturer's instructions (Roche, Germany).

Animals. The production, genotyping, and background strain (C57BL/6 × SJL) of Tg2576 mice used in this study were previously described (13). Tg2576 mice harboring the mutated human APP695 gene including the Swedish double mutation (K670N/M671L) were obtained from Taconic (Germantown, NY).

Immunohistochemistry. AD and age-matched control brains were obtained from the autopsy service at University of Oklahoma Heath Sciences Center and Korea Scientific Investigation Center. A neuropathological diagnosis of AD was confirmed according to the criteria of Braak and Braak (6). Blocks of AD or control tissues were fixed in 10% neutral buffered formalin for 48 h. After fixation, the brain tissue was dehydrated and embedded in paraffin. Immunohistochemistry was performed using a Vectastain avidin-biotin complex elite kit (Vector, Burlingame, CA) as described previously (19). Images were captured using an optical microscope (BX51TF; Olympus Optical Co., Japan) equipped with an exposure control unit (PM-CB20) and a camera (CPM-C35DX).

The Tg2576 mouse brains ($n = 5$), fixed in 10% neutral buffered formalin for 48 h, were dehydrated and embedded in paraffin. Fluorescent immunohistochemistry was performed with appropriate primary antibodies for 2 h and visualized using Cy3-conjugated or fluorescein isothiocyanate-conjugated secondary antibody (Jackson, West Grove, Pennsylvania). 4′,6′-Diamidino-2-phenylindole (DAPI) counterstaining was performed. Images were collected using the laser scanning microscope (LSM) 510 program on a Zeiss confocal microscope.

Evaluation of apoptosis with TUNEL staining. Apoptosis was assessed using the In Situ Cell Death Detection kit (Roche) according to the manufacturer's instructions. The numbers of terminal deoxynucleotidyltransferase-mediated dUTP-biotin nick end labeling (TUNEL)-positive cells in four random fields were quantified as an index of apoptosis and were normalized as percent ratios versus the total number of cells showing AICD-GFP fluorescence.

FRET measurements. Fluorescent resonance energy transfer (FRET) measurements were observed using a Zeiss LSM 510 confocal microscope mounted on a Zeiss Axiovert 200 inverted microscope; the krypton-argon laser (emission, 488- and 543-nm lines) was used to excite the enhanced GFP (EGFP) and Cy3, respectively, as described previously (18). Briefly, EGFP-expressing (donor) cells were labeled with acceptor-conjugated molecules (Cy3), and energy transfer was detected as an increase in donor fluorescence (dequenching) after complete photobleaching of the acceptor molecule (Cy3). EGFP was excited with the 488-nm line of an argon laser, and the red fluorophores were excited with a helium/neon laser emitting at 543 nm. Tracks were scanned sequentially with only one laser and the respective detector channel active per scan. FRET was calculated from the increase in donor fluorescence after acceptor photobleaching by relative fluorescence intensity (%).

Immunoprecipitation. One hundred micrograms of sample in 1 ml of lysis buffer was incubated with 1 μg of primary antibody with rotation for 1 h at 4°C, treated with protein G Plus/protein A-agarose (Oncogene, California) for 1 h at 4°C, and centrifuged at 14,000 rpm for 20 min. The pellets obtained were washed three times with 1 ml of lysis buffer, boiled for 5 min with sample buffer (0.2 M Tris-HCl, pH 6.8, 10% sodium dodecyl sulfate [SDS], 25% glycerol, and 0.01% bromophenol blue), and then centrifuged at 13,000 rpm for 15 min. The supernatants were subjected to SDS-polyacrylamide gel electrophoresis.

Western blotting. Protein was resolved in an SDS-polyacrylamide gel, electrophoresed at 30 to 50 μg of protein/lane, and transferred onto a nitrocellulose membrane (Amersham Pharmacia, Buckinghamshire, United Kingdom). The protein blot was confirmed with appropriate antibodies and detected using horseradish peroxidase-conjugated secondary antibody (Amersham Pharmacia). Immunoreactive bands were visualized using an enhanced chemiluminescence system (Amersham Pharmacia, Buckinghamshire, United Kingdom).

Nuclear and cytoplasmic fractionation. At 48 h posttransfection, PC12 cells or primary neurons plated on six-well plates were washed with ice-cold phosphate-buffered saline, and then nuclear and cytoplasmic fractionation was performed according to the manufacturer's protocol (nuclear and cytoplasmic extraction reagents; Pierce, Illinois).

The cerebral cortex and hippocampal regions were dissected from the brains isolated from Tg2576 mice or wild-type (WT) mice. The dissected tissues (100 mg) were rinsed twice with phosphate-buffered saline buffer and resuspended with 1 ml of 1× lysis buffer (100 mM HEPES, pH 7.9, 15 mM $MgCl_2$, 100 mM KCl) containing dithiothreitol and protease inhibitors. Then the tissues were homogenized for 3 to 5 min, and the disrupted tissues were centrifuged for 10 min at 400 × *g*. The supernatant was transferred to a fresh tube, and after a centrifugation for 10 min at 1,500 × *g*, the resultant supernatant was collected as the cytoplasmic fraction. The nuclear pellet was washed in 1 ml of 1× lysis buffer for 10 min at 1,500 × *g*, and the supernatant was discarded. The crude nuclear pellet was resuspended in 140 μl of extraction buffer (20 mM HEPES, pH 7.9, 1.5 mM $MgCl_2$, 0.42 M $NaCl_2$, 0.2 mM EDTA, 25% [vol/vol] glycerol) containing dithiothreitol and protease inhibitors, and the resuspended nuclei were centrifuged for 3 h at 20,000 × *g*. The supernatant was transferred to a clean, prechilled tube. This extraction is the enriched nuclear fraction.

Luciferase assay. For transactivation by APP-Gal4, cells were cotransfected, where indicated, with one of the following: (i) pG5E1B-luc (Gal4 reporter plasmid); (ii) pMst (Gal4), pMst-APP (APP-Gal4), pMst-T668A APP (APP^{T668A}-Gal4), pMst-AICD (AICD-Gal4), and pMst-T668A AICD (AICD^{T668A}-Gal4); or (iii) pcDNA3-Fe65 (Fe65). Analyses were performed as described previously (8).

Human GSK-3β promoter (nucleotides [nt] −2090 to ~+1035) in pCAT vector was a kind gift from P. C. Shaw at the Chinese University of Hong Kong. The promoter region in the vector was excised at the KpnI and BglII sites and inserted into the KpnI and BglII sites of the PGL2 promoter plasmid (Promega, Wisconsin). For cotransfection experiments, 4 μg of human GSK-3β promoter in PGL2 vector and AICDs (C50, dC50, or C50^{T668A}) in pEGFP-N1 vector was added to the PC12 cells. Luciferase activity was measured using a Biocounter M1500 luminometer (Lumac, GE, Groningen, The Netherlands). Protein concentrations were determined using the Bradford protein assay reagent (Bio-Rad), and luciferase activities were normalized versus the obtained protein concentrations.

Statistical analysis. Data are represented as means ± standard errors of the means. Analysis of variance (ANOVA) tests were used to study the relationships

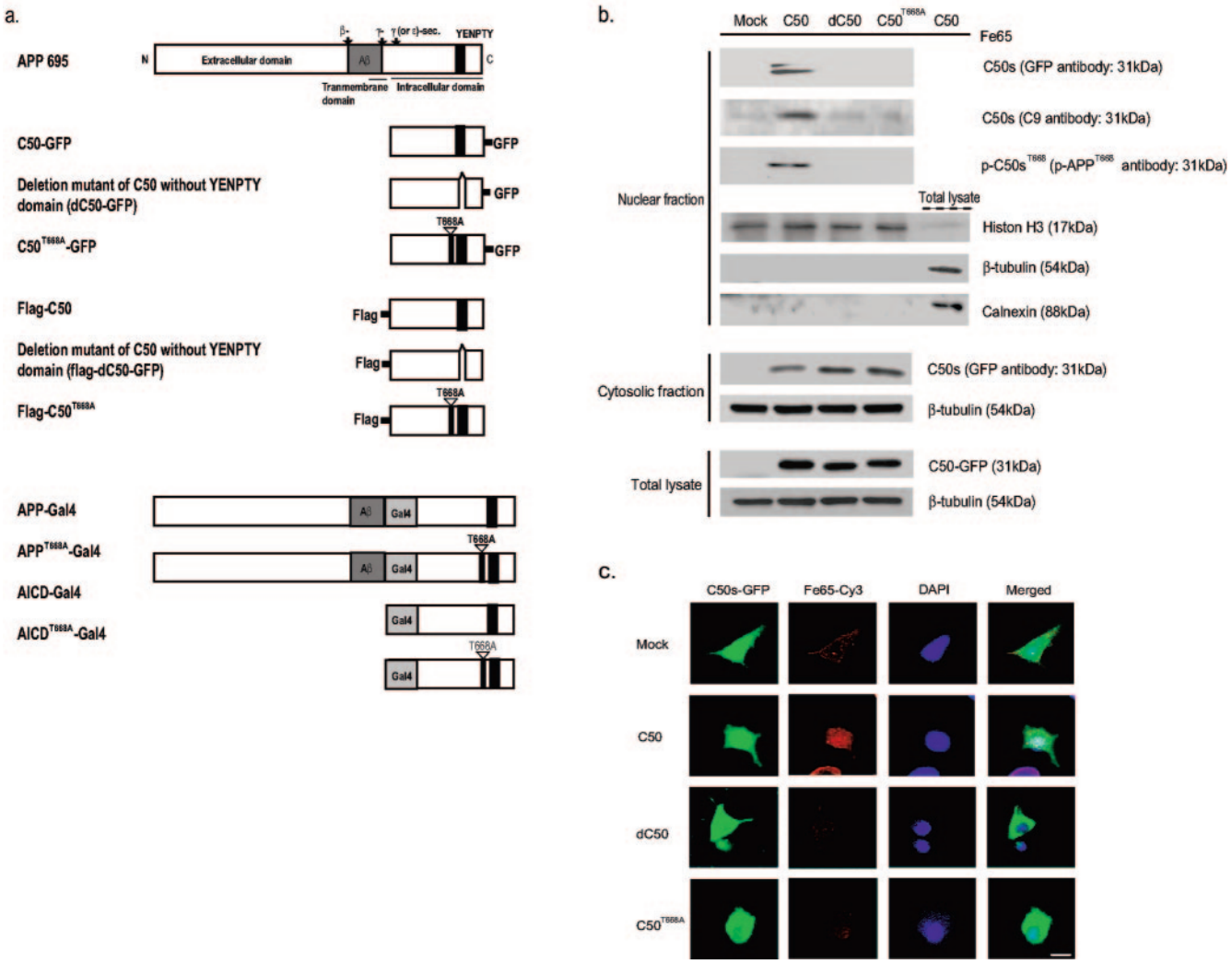

FIG. 1. Phosphorylation of the AICD at T668 is required for its nuclear translocation. (a) Schematic representations of the AICD (C50) and mutated forms of C50 (dC50, $C50^{T668A}$) used in this study are shown. The C50 construct was generated by PCR from human APP695 cDNA to encompass the last 50 amino acid residues. It was subcloned into a pcDNA3-flag vector with the flag at the N terminus, into a pEGFP-N1 vector with GFP at the carboxyl terminus, or into a pMst vector with Gal4. Mutagenesis of the YENPTY deletion or T668A mutant variants in the C50 construct was achieved using a QuikChange site-directed mutagenesis kit (Stratagene, La Jolla, California). (b) The presence of the AICDs was examined in the nuclear and cytosolic fractions of C50, dC50, $C50^{T668A}$ expressing NGF-differentiated PC12 cells using anti-GFP or C9 antibodies. The purity of nuclear fractions was confirmed by Western blotting using anti-histone H3 (nucleus marker), anti-β-tubulin antibody (a cytosolic marker), and anti-calnexin (an endoplasmic reticulum marker). (c) Differentiated PC12 cells were cotransfected with the AICDs in pEGFP-N1 vector and Fe65 in pcDNA3-flag vector. At 48 h posttransfection, immunocytochemical experiments were performed to investigate the colocalization of AICDs with Fe65. DAPI (1 μM) staining indicates the location of the nucleus (blue). GFP fluorescence shows green fluorescence representing the location of AICDs. Cy3 fluorescence shows the location of Fe65 in the pcDNA3-flag vector (red) by anti-flag antibody, conjugated by Cy3-labeled secondary antibody. Panels on the right are merged images. Bar, 10 μm.

between variables. The difference was considered statistically significant when the P value was ≤ 0.05 or ≤ 0.01.

RESULTS

Phosphorylation at T668 is required for interaction with Fe65 and translocation of AICD into the nucleus. Under our experimental conditions, the efficiencies of the transient transfections of APP-CTFs cloned in either pEGFP-N1 or pcDNA3-flag vector using Fugene 6 were 40.0% ± 4.0% (pEGFP-N1 vector, $n = 5$) and 37.5% ± 6.0% (pcDNA-3 flag vector, $n = 15$) for differentiated PC12 (dPC12) cells and 19.5% ± 3.0% (pEGFP-N1 vector, $n = 5$) and 19.3% ± 5.1% (pcDNA-3flag vector, $n = 5$) for rat primary cortical neurons, as confirmed by the expression of GFP fluorescence or immunocytochemical experiments using anti-flag antibody.

In this study, we focused on the effects of phosphorylation at T668 in the translocation of AICD (C50) into the nucleus based on the hypothesis that T668 phosphorylation may affect the translocation of AICD by causing a significant conformational change, altering the interaction with binding partners. Initially, we checked whether the AICD is detected in the nucleus after transfecting cells with C50, the deletion mutant

of C50 without the YENPTY domain (dC50), and the T-668-A mutant of C50 ($C50^{T668A}$) cloned in pEGFP-N1 or pcDNA3-flag vector (Fig. 1b). At 48 h posttransfection, we found that AICD, detected by anti-GFP or C9 antibody, was present in the nuclear fractions of C50-transfected dPC12 cells but not in the cells expressing dC50 or $C50^{T668A}$. In the cytosolic fraction of AICD mutant-transfected dPC12 cells, dC50 or $C50^{T668A}$ was dominantly detected and a little AICD was found. We also found that a large portion of phosphorylated AICD at T668 was detected in the nuclear fraction of dPC12 cells expressing C50. These results indicate that the phosphorylated form of C50 at T668 was dominantly translocated into the nucleus. The purity of the nuclear fraction was confirmed with subcellular marker proteins in the proper fractions: calnexin for ER, tubulin for cytosol, and histone H3 for nucleus (Fig. 1b).

We wanted to confirm whether the AICD interacts with Fe65 and whether this interaction is necessary for translocation into the nucleus to perform nuclear functions (8). To address this issue, we investigated the subcellular location of C50, dC50, or $C50^{T668A}$ by confocal immunofluorescence microscopy and determined whether they colocalized with Fe65 in NGF-dPC12 cells. In the cells expressing C50-GFP, we found that the GFP signal was found to colocalize with Fe65 in the nucleus (Fig. 1c). In contrast, the GFP signal in the cells expressing mock, dC50, or $C50^{T668A}$ was mainly detected in the cytoplasm (Fig. 1c). We also found that Cy3 immunofluorescence representing Fe65 in the pcDNA3-flag vector was colocalized with the C50-GFP signal in the nucleus of C50-transfected cells but not in dC50- or $C50^{T668A}$-transfected cells (Fig. 1c).

Next, to further clarify whether the phosphorylated AICD (C50) at T668 binds to Fe65 in the nucleus, FRET analysis was performed. In C50-EGFP- and Fe65-transfected cells labeled with monoclonal Fe65 antibody (Cy3), EGFP and Cy3 signals were found to be colocalized in the nucleus (Fig. 2). The amount of FRET was calculated as the percentage of increase in donor fluorescence (EGFP) at 488 nm after acceptor (Cy3) photobleaching at 514 nm. As shown in Fig. 2b, in the cells coexpressing C50 and Fe65, the GFP donor signal at 488 nm was significantly increased by 154.82 ± 19.94 ($P < 0.05$; $n = 4$) after photobleaching of the Cy3 signal at 514 nm, indicating that FRET is present between C50-GFP and Fe65-Cy3. By contrast, FRET was not observed between EGFP (mock)- and Fe65-transfected cells (Fig. 2a). In addition, we found that FRET did not occur between Fe65 and $C50^{T668A}$, suggesting that T668 phosphorylation is critically required for the interaction between C50 and Fe65 (Fig. 2c). Our FRET data clearly show that the presence of phosphorylation of AICD at T668 is necessary for the binding of AICD and Fe65.

AICD induces GSK-3β expression and tau phosphorylation in NGF-differentiated PC12 cells and rat primary cortical neurons, whereas the T668A point mutant does not. Previously, Fe65 binding to APP was reported to activate its transcriptional activity (8). In this investigation, we tested the effects of T668A mutation on the transcriptional activity of APP and AICD. Here, we found that the transactivations of their T668A mutants (APP^{T668A}-Gal4 and $AICD^{T668A}$-Gal4) cotransfected with Fe65 show much less significant increases (approximately a 20-fold induction) compared to APP-Gal4 or AICD-Gal4 cotransfected with Fe65 (e.g., >100-fold versus Gal4) (Fig. 3a). In addition, single transfections with APP-Gal4 or AICD-Gal4 constructs could not stimulate transactivation (approximately a twofold induction) (Fig. 3a).

To elucidate whether phosphorylation of AICD affects its interaction with Fe65 and CP2, we performed a coimmunoprecipitation assay. Compared with wild-type C50, $C50^{T668A}$ showed a significantly decreased interaction with Fe65 and CP2 (Fig. 3b). Weak bands representing the presence of phosphorylated C50 shown in $C50^{T668A}$- or dC50-expressing cells seem to show the presence of endogenous AICD phosphorylated at T668. In addition, the weak bands indicating the interaction with Fe65 and CP2 are thought to be due to the endogenous AICD phosphorylated at T668. Immunoprecipitation using preimmune serum revealed that these interactions were specific (data not shown). These results showed that the AICD-Fe65-CP2 ternary complex existed in the nucleus of C50-transfected dPC12 cells and that the interactions among these three proteins are affected both by phosphorylation at T668 and by the presence of the YENPTY domain.

We also examined whether the phosphorylation of AICD (C50) at T668 affected GSK-3β expression or tau phosphorylation in dPC12 cells and in rat primary cortical neurons. We found significant increases in GSK-3β expression and tau phosphorylated at Ser^{202} and Thr^{205} in C50-transfected cells but no increase in the deletion mutant or in T668A mutant-transfected cells (Fig. 3c).

We also found an increase in GSK-3β promoter activity in C50-transfected dPC12 cells but no increase in the case of the T668A point mutation (Fig. 3d). Additionally, the deletion of the CP2 binding site (−1 to +10) in the human GSK-3β promoter completely inhibited increased promoter activity by C50, whereas the deletion of the CP2 binding site (−1292 to −1282) partially reduced the increased GSK-3β promoter activity by C50 (Fig. 3d).

Treatment with cdc2 kinase, cdk5, or GSK-3β inhibitors decreases the cell death induced by the AICD. Here, we examined whether treatment with inhibitors of the kinases known to be responsible for T668 phosphorylation affected the GSK-3β induction and tau phosphorylation induced by C50 expression in dPC12 cells and in rat primary cortical neurons. We first confirmed that treatment with 40 μM olomoucine (a cdc2 kinase inhibitor), 5 μM roscovitine (a cdk5 inhibitor), or 10 mM LiCl (a GSK-3β inhibitor) for 48 h significantly reduced the phosphorylated form of C50 at T668, GSK-3β expression, tau phosphorylation induced by C50 (Fig. 4a), and GSK-3β promoter activity induced by C50 (Fig. 4b). We also checked the effects of the treatment of three kinase inhibitors (olomoucine, roscovitine, and LiCl) on the nuclear translocation of the AICD. Differentiated PC12 cells were cotransfected with the AICD in the pEGFP-N1 vector and Fe65 in the pcDNA3 flag vector. The transfected cells were incubated in the presence or absence of one of three kinase inhibitors (40 μM olomoucine, 5 μM roscovitine, or 10 mM LiCl) for 48 h. Then the presence of the AICD was detected with anti-GFP antibody or anti-$pAPP^{T668}$ antibody which specifically recognizes phosphorylated APP at T668 in nuclear fractions of the cells. AICD and phosphorylated AICD at T668 were found to be more abundantly detected when treated with vehicles only, whereas a much lower amount of the AICD was observed in nuclear fractions when these were treated with one of the three

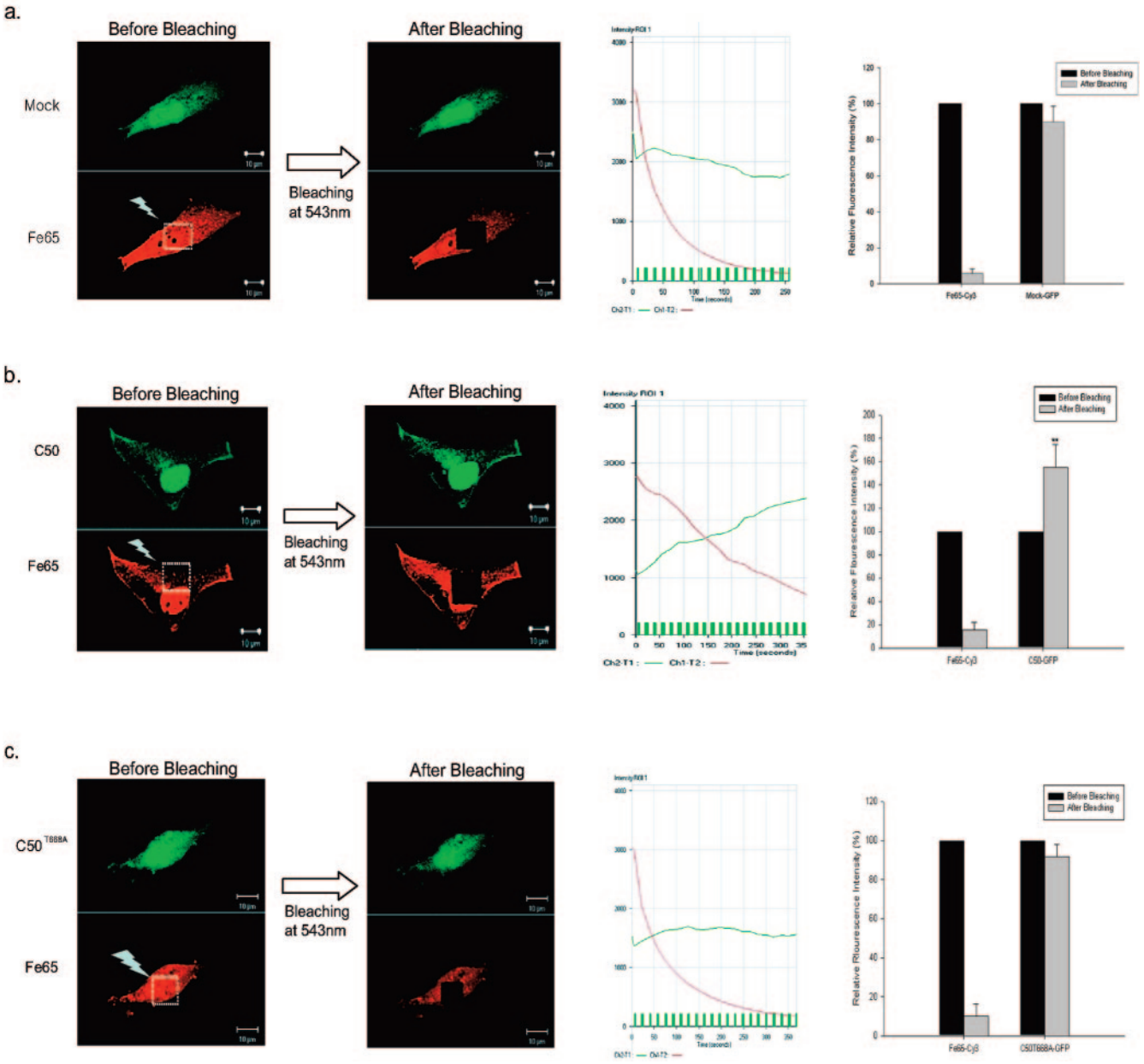

FIG. 2. Molecular interaction between the AICD and Fe65 factor examined by FRET. (a, b, and c) Quantitative FRET analysis using acceptor bleaching in SK-N-SH cells cotransfected with Fe65 and mock (a), C50 (b), or $C50^{T668A}$-EGFP (c) expression constructs. Cells were immunostained with anti-Fe65 antibody and visualized with Cy3. Left panels, EGFP signal (mock, C50, or T668A C50) using 488-nm excitation and Cy3 (Fe65) signal using 543-nm excitation before photobleaching and EGFP signal (mock, C50, or T668A C50) using 488-nm excitation and Cy3 (Fe65) signal using 543-nm excitation after photobleaching of the acceptor (Cy3) fluorophore with intense 543-nm laser light (white rectangle). Bar, 10 μm. Middle panels, intensity of the region of interest (ROI), quantification of fluorescence intensity in a representative example also shows a substantial increase in fluorescence after the bleach only in the C50-transfected cells. Right panels, graphs show the percentages of relative fluorescence intensity. Data represent means ± standard errors of results from four separate experiments. **, $P < 0.01$; *, $P < 0.05$ (by ANOVA).

kinase inhibitors (Fig. 4c). In addition, decreased cell viability by C50 was overcome by treating each of the three kinases (data not shown), suggesting that the phosphorylation of C50 at T668 is critical for inducing GSK-3β expression, which leads to increased tau phosphorylation and neurotoxicity. Indirubin 3′-monoxime, 5-iodo, a GSK-3β inhibitor, was effective in restoring the cell viability at 9 nM in which GSK-3β activity is specifically inhibited, while the inactive analogues of olomoucine and LiCl, respectively, iso-olomoucine (100 μM) and NaCl (10 mM), had no effect (data not shown). These results clearly show that all of these kinase inhibitors are effective in attenuating the cytotoxicity induced by AICD by specifically acting on the enzymes responsible for phosphorylation of T668: cdc2, cdk5, and GSK-3β.

T668A mutation significantly reduces the apoptotic cell death induced by the AICD. We examined whether the phos-

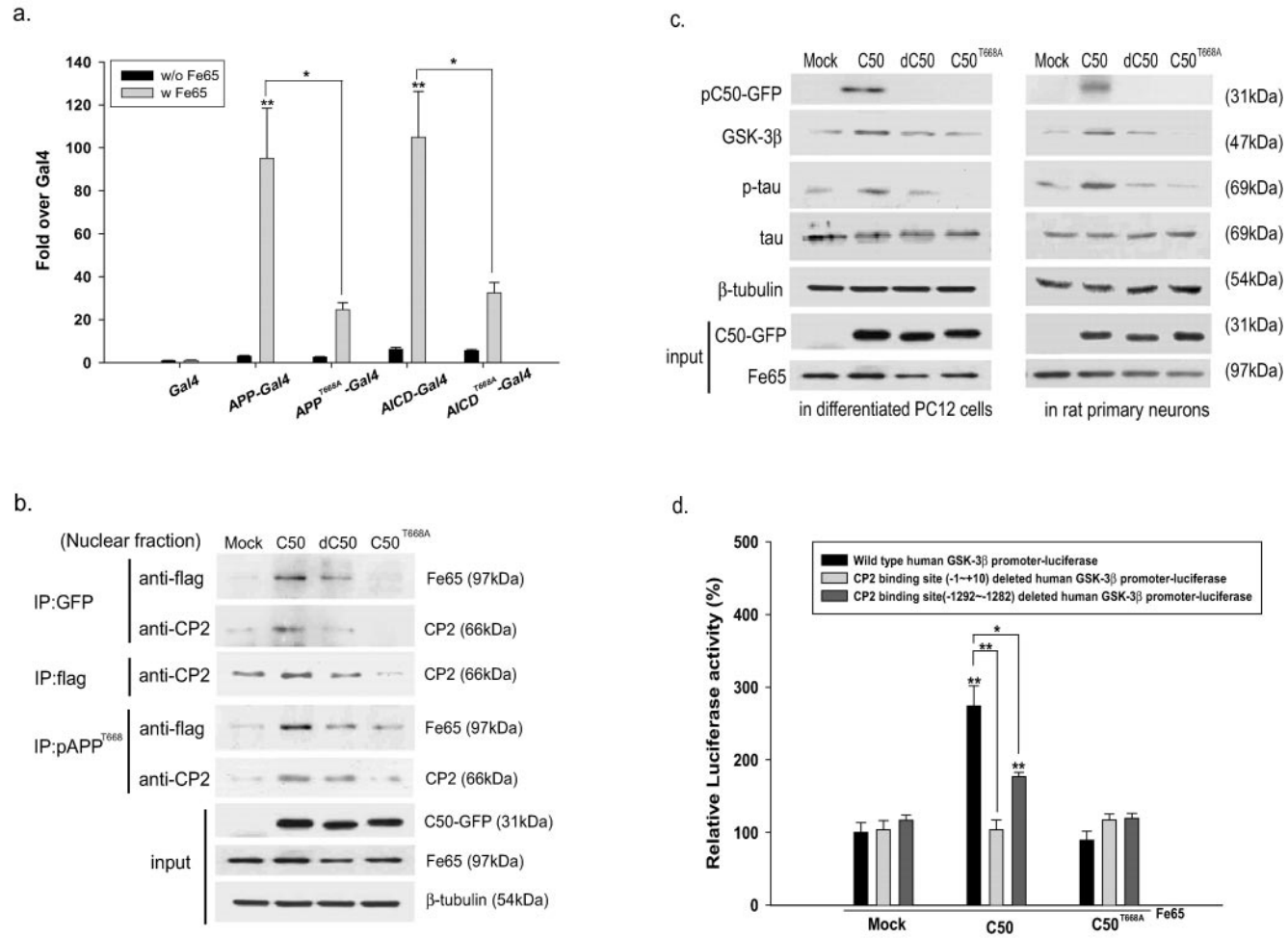

FIG. 3. The AICD induces GSK-3β expression and tau phosphorylation in NGF-differentiated PC12 cells and rat primary cortical neurons, whereas the T668A point mutant does not. (a) For transactivation by APP-Gal4, cells were cotransfected with one of the following: (i) pG5E1B-luc (Gal4 reporter plasmid); (ii) pMst (Gal4), pMst-APP (APP-Gal4), pMst-T668A APP (APP^{T668A}-Gal4), pMst-AICD (AICD-Gal4), and pMst-T668A AICD ($AICD^{T668A}$-Gal4); or (iii) pcDNA3-Fe65 (Fe65). Analyses were performed as described previously (8). The normalized luciferase activity is expressed as the relative induction over transcription by Gal4 alone. (b) To confirm the interactions between AICDs, Fe65, and CP2, we performed immunoprecipitation and immunoblotting. After immunoprecipitation with each indicated antibody (anti-GFP, anti-flag, or anti-$pAPP^{T668}$ antibody), immunoblotting was performed using the nuclear fraction obtained from differentiated PC12 cells cotransfected with ACIDs and Fe65 using antibodies against Fe65 or CP2. The expression levels of AICDs in the pEGFP-N1 vector and Fe65 in differentiated PC12 cells were checked using anti-GFP or anti-flag antibodies. (c) At 48 h posttransfection, the changes in GSK-3β protein and p-tau were checked by Western blotting with anti-GSK-3β or AT8 antibody, which recognizes phosphorylated tau at its Ser^{202} and Thr^{205} sites, in PC12 cells and rat primary cortical neurons cotransfected with AICDs and Fe65. The level of total tau protein was checked as well as that of β-tubulin. The expression levels of AICDs in pEGFP-N1 vector and Fe65 in differentiated PC12 cells were checked using anti-GFP antibody or anti-Fe65 antiserum. (d) GSK-3β promoter activity was measured by luciferase activity assay in PC12 cells cotransfected with AICDs and human GSK-3β promoter in PGL2 vector. For cotransfection experiments, 4 μg of human GSK-3β promoter in PGL2 vector and AICDs (C50, dC50, or $C50^{T668A}$) in pEGFP-N1 vector were added to dPC12 cells. Luciferase activity was measured using a Biocounter M1500 luminometer (Lumac, GE, Groningen, The Netherlands). Protein concentrations were determined using Bradford protein assay reagent (Bio-Rad), and luciferase activities were normalized versus the obtained protein concentrations.

phorylation of C50 at T668 played a role in inducing apoptotic cell death in neuronal cells. The mean ± standard error cumulative apoptotic indexes of mock-, C50-, dC50-, and $C50^{T668A}$-transfected cells at 48 h posttransfection compared to transfected total cells were 7.7% ± 0.6%, 30.0% ± 0.4%, 21.0% ± 0.4%, and 18.5% ± 0.4%, respectively (Fig. 5a, b). We found that deletion mutants (dC50) which do not have a YENPTY domain and T668A mutants ($C50^{T668A}$) displayed fewer apoptotic nuclei than those transfected with C50, suggesting that apoptotic cell death induced by the AICD is related both to phosphorylation at T668 and to the YENPTY domain.

Next, by lactate dehydrogenase (LDH) release assay, we evaluated the viabilities of dPC12 cells and rat primary cortical neurons transfected with C50. After 48 h posttransfection, cells expressing C50 showed significantly increased LDH release (about 30%) versus mock-transfected controls in dPC12 cells and rat primary cortical neurons, but LDH release was significantly reduced to the level of the mock control in YENPTY

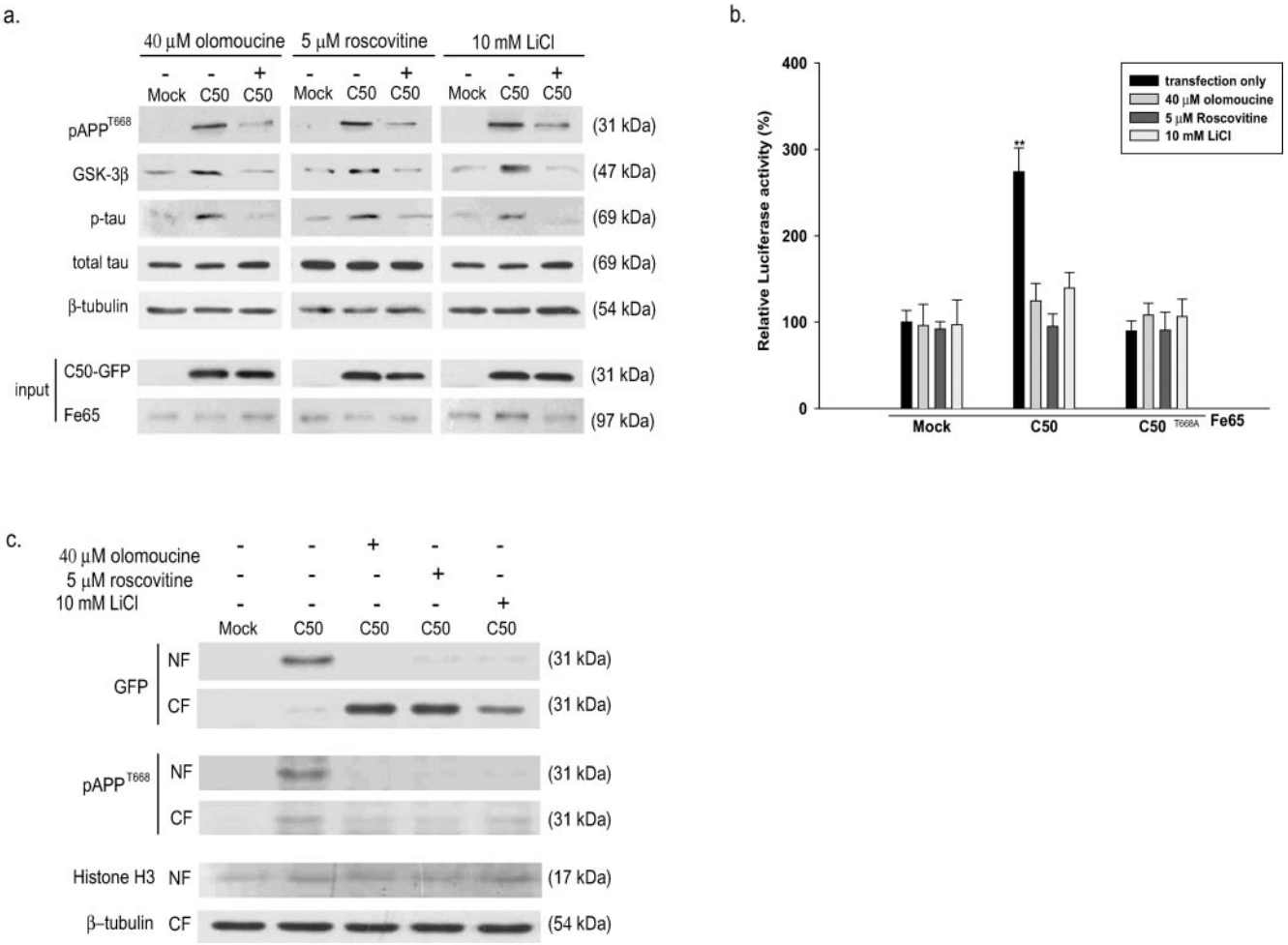

FIG. 4. Inhibitors of phosphorylation at T668 significantly decrease the induction of GSK-3β induced by the AICD in differentiated PC12 cells. (a) At 48 h posttransfection, the protein levels of pC50^{T668}, GSK-3β, and p-tau were examined by Western blotting after treatment with three kinase inhibitors, olomoucine (40 μM), roscovitine (5 μM), and LiCl (10 mM) in dPC12 cells. (b) GSK-3β promoter activity after treatment with olomoucine, roscovitine, or LiCl was measured by luciferase activity assay in dPC12 cells. (c) At 48 h posttransfection, the protein levels of C50 and pC50^{T668} were examined in the nuclear fraction (NF) and the cytoplasmic fraction (CF) by Western blotting after treatment with three kinase inhibitors, olomoucine (40 μM), roscovitine (5 μM), and LiCl (10 mM), in dPC12 cells. Data represent the means ± standard errors of the means of results from four separate experiments. *, $P < 0.05$; **, $P < 0.01$ (by ANOVA).

deletion mutant-transfected cells and in T668A mutant-transfected cells (data not shown).

APP-CTFs phosphorylated at T668, GSK-3β, and p-tau were increased in AD and Tg mouse brains. We initially examined the expression of p-APP^{T668} in human AD brains and in Tg2576 mouse brains. More intense staining of p-APP^{T668} was observed in hippocampal pyramidal neurons and in neurons of the dentate gyrus and ectorhinal cortex of AD brains (Braaks stage V) (6) than was observed in age-matched controls (Fig. 6a). The immunoreactivities of APP-CTFs were increased in the serial sections of AD brain regions using C9 antibody which specifically recognizes the APP C terminus (data not shown). Both in transfected cells (22) and in vivo (12, 23), GSK-3β has been known to phosphorylate tau in most hyperphosphorylated sites in paired helical filaments (PHFs). Immunostaining for GSK-3β and for p-tau showed that its immunoreactivities were widely distributed in the neurons of the AD brains, but little immunoreactivity was found to be present in comparable regions of the brains of age-matched controls (Fig. 6b, c). The protein level of GSK-3β was confirmed in total lysates from normal age-matched brains and AD brains by Western blot analysis. We found significant increases in GSK-3β expression in total lysates from AD brains (Fig. 6b).

In Tg2576 mouse brains, immunoreactivities for p-APP^{T668}, GSK-3β, and p-tau were significantly increased in the CA1 and CA3 hippocampal regions (Fig. 7a, b). In particular, immunoreactivities against p-APP^{T668} were observed in the nucleus (Fig. 7a, b). However, few of these immunoreactivities were seen in comparable regions of WT mouse brains. Using hematoxylin and eosin staining, we confirmed the increase of degenerating neurons in the serial sections of Tg2576 mouse brain tissues (data not shown). In brain lysates of the cortex and hippocampus of Tg2576 mouse brains, levels of AICD, CTFs, phosphorylated AICD, and phosphorylated CTFs were checked (Fig. 7c, d). Then we normalized total APP-CTFs

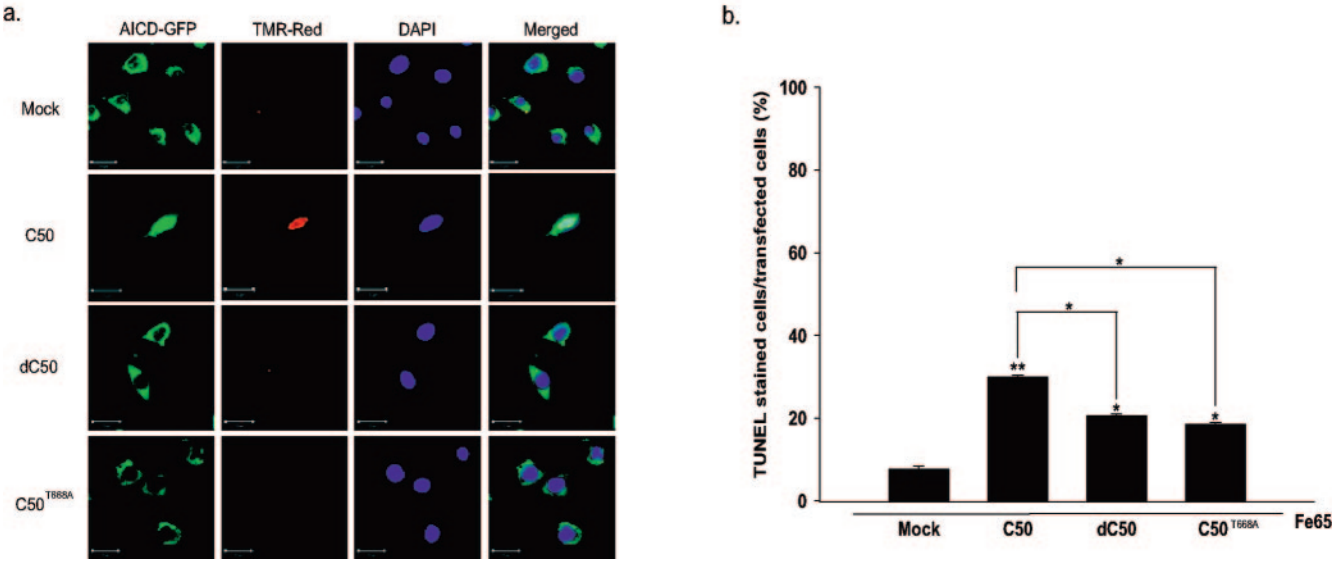

FIG. 5. T668A mutation significantly decreases neuronal cell death induced by AICD. The constructs of mock, C50, dC50, and $C50^{T668A}$ in pEGFP-N1 vector were cotransfected with Fe65 into dPC12 cells. (a) TUNEL-stained sections of transfected dPC12 cells. GFP, GFP fluorescent images of AICD-GFP; TMR-Red, TUNEL-stained images; DAPI, DAPI-stained images; merged, merged images. Bar, 20 μM. (b) The percentage of TUNEL-positive cells of transfected dPC12 cells. Data represent the means ± standard errors of results from four separate experiments. **, $P < 0.01$; *, $P < 0.05$ (by ANOVA).

versus total full-length APP and examined their T668 phosphorylation levels to compare T668 phosphorylation levels in Tg2576 mice versus WT mice. Here we found that phosphorylated APP-CTFs were much more increased in Tg2576 mouse brains than in WT mice, suggesting that T668 phosphorylation might be a contributing factor to AD pathology in this AD animal model (Fig. 7c, d). In addition, AICD was detected in the nuclear fractions of the cortex of Tg2576 mouse brains using C9 antibody which specifically recognizes the APP C terminus (Fig. 7e). We also found that more-intense GSK-3β bands were detected in the cortex of APP transgenic mouse brains than in that of WT mouse brains (Fig. 7f).

DISCUSSION

Recent studies have shown that the intracytoplasmic APP-CTFs (including the AICD) may be involved in the pathogenesis of AD. It is reported that the AICD stabilized by its association with Fe65 is transported into the nucleus and has a transcriptional activity (8, 15, 16, 38). KAIi, GSK-3β, APP, BACE1, Tip60, and neprilysin have been reported as target genes whose expression is regulated by Fe65 and AICD (4, 15, 24, 35, 38).

Here we report that the phosphorylation of AICD at T668 is required for the translocation of AICD into the nucleus and induces neurotoxicity, possibly mediated through the induction of GSK-3β and tau phosphorylation by enhancing the formation of a ternary complex with Fe65 and CP2 transcription factor.

APP is constitutively phosphorylated at T668 in brain tissues and neuronal cells (14), and stress stimulus can induce this phosphorylation even in nonneuronal cells (34). Several physiological functions of phosphorylated APP have been proposed: phosphorylated APP is largely localized in the neurite tips of neuronal cells which can play important role in axonal guidance (2, 14). Also, T668 phosphorylation was reported to play a role in APP metabolism by facilitating the BACE cleavage of APP to increase Aβ generation (21). However, the roles and the physiological functions of the phosphorylation of APP or the AICD at T668 remain largely unknown.

In the present study, we show that the phosphorylation of the AICD at T668 is required for its binding to Fe65 and phosphorylated AICD dominantly translocates into the nucleus. Our FRET data clearly indicate that the phosphorylation of AICD is essential for its binding to Fe65, and we could detect phosphorylated AICD in the nuclear fraction of cells cotransfected with AICD and Fe65. These results were confirmed by using specific inhibitors for cdc2, GSK-3β, and cdk5 kinases known to responsible for T668 phosphorylation or mutations of T668 sites (T668A). The inhibition of phosphorylation at T668 significantly reduced the translocation of AICD into the nucleus and the transcriptional activities of Gal4-APP constructs. Also, the cytotoxicity induced by the AICD (C50) was significantly reduced by the inhibition of phosphorylation at T668.

Fe65, one of the known adaptor proteins bridging APP to specific molecular pathways (11), contains three protein-protein interaction domains, a WW domain and two PTB domains. The PTB2 domain, located in the C-terminal half of the molecule, is responsible for the interaction of Fe65 (26) with the cytosolic tail of APP through the YENPTY domain, located between amino acids 682 and 687 (using APP695 numbering) (5, 41). Fe65 has also been reported to bind the CP2/LSF/LBP1 family transcription factor through the PTB1 domain (41). Numerous results demonstrated that this protein was a housekeeping factor regulating GSK-3β (20) of a varied array of genes.

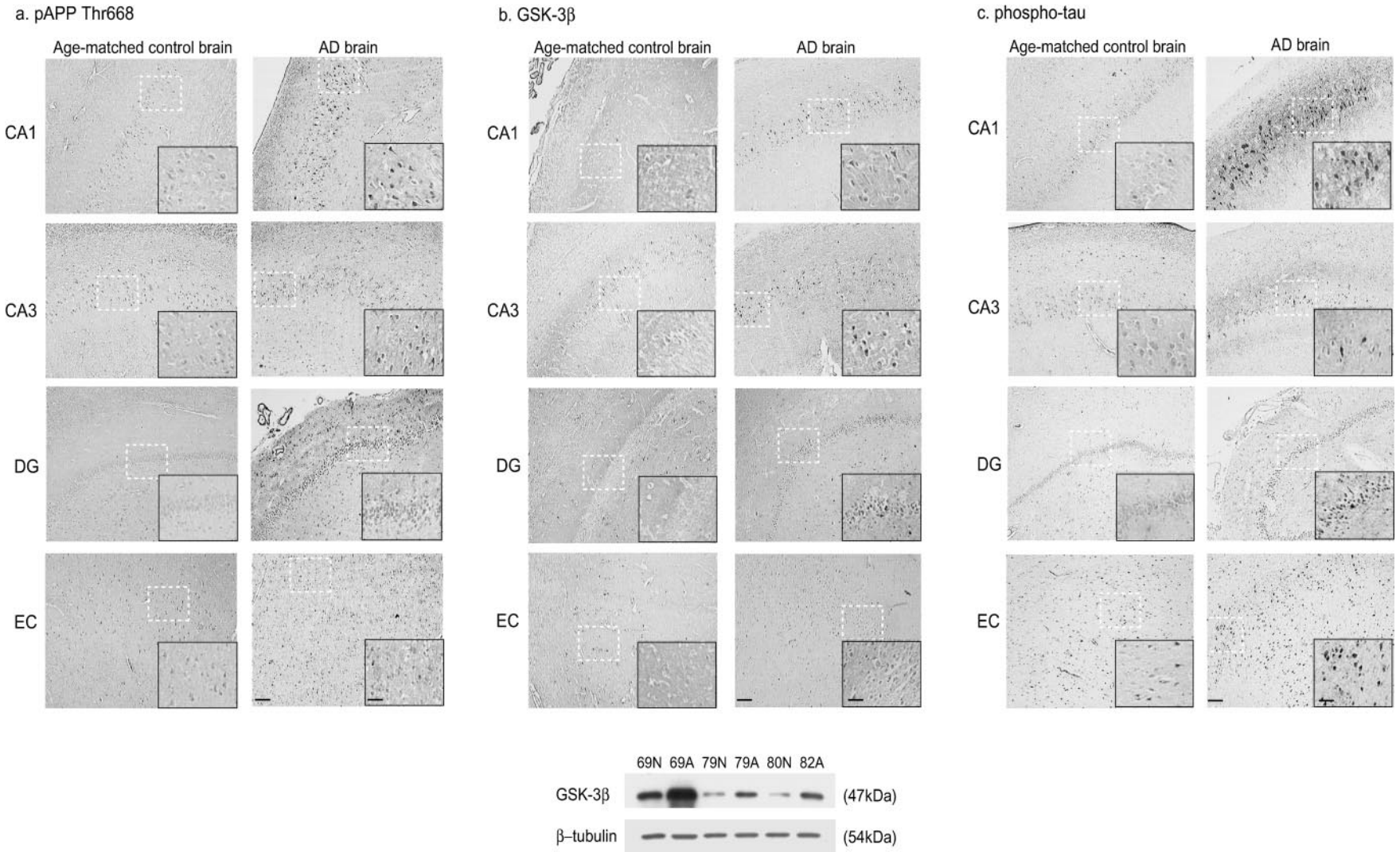

FIG. 6. pAPP^{T668}, GSK-3β, and p-tau are upregulated in AD brains. Immunoreactivities of phosphorylated APP-CTFs at T668 (using pAPP^{T668} antibody) (a), GSK-3β (using anti-GSK-3β antibody) (b), and p-tau (using AT8 antibody) (c) were examined in the hippocampus (CA1, CA3), dentate gyrus (DG), and ectorhinal cortex (EC) of an AD brain and a normal age-matched brain using pT668 antibody. Bars, 250 μm (lower-magnitude photographs [magnification, ×34.4]). The inserts show higher magnifications of the stained sections (magnification, ×172). Bars, 50 μm. (Bottom) Immunoblot analysis of GSK-3β and β-tubulin using the hippocampus of normal age-matched brains and AD brains: 69N, 69-year-old normal control brain; 69A, 69-year-old AD brain; 79N, 79-year-old normal control brain; 79A, 79-year-old AD brain; 80N, 80-year-old normal control brain; 82A, 82-year-old AD brain.

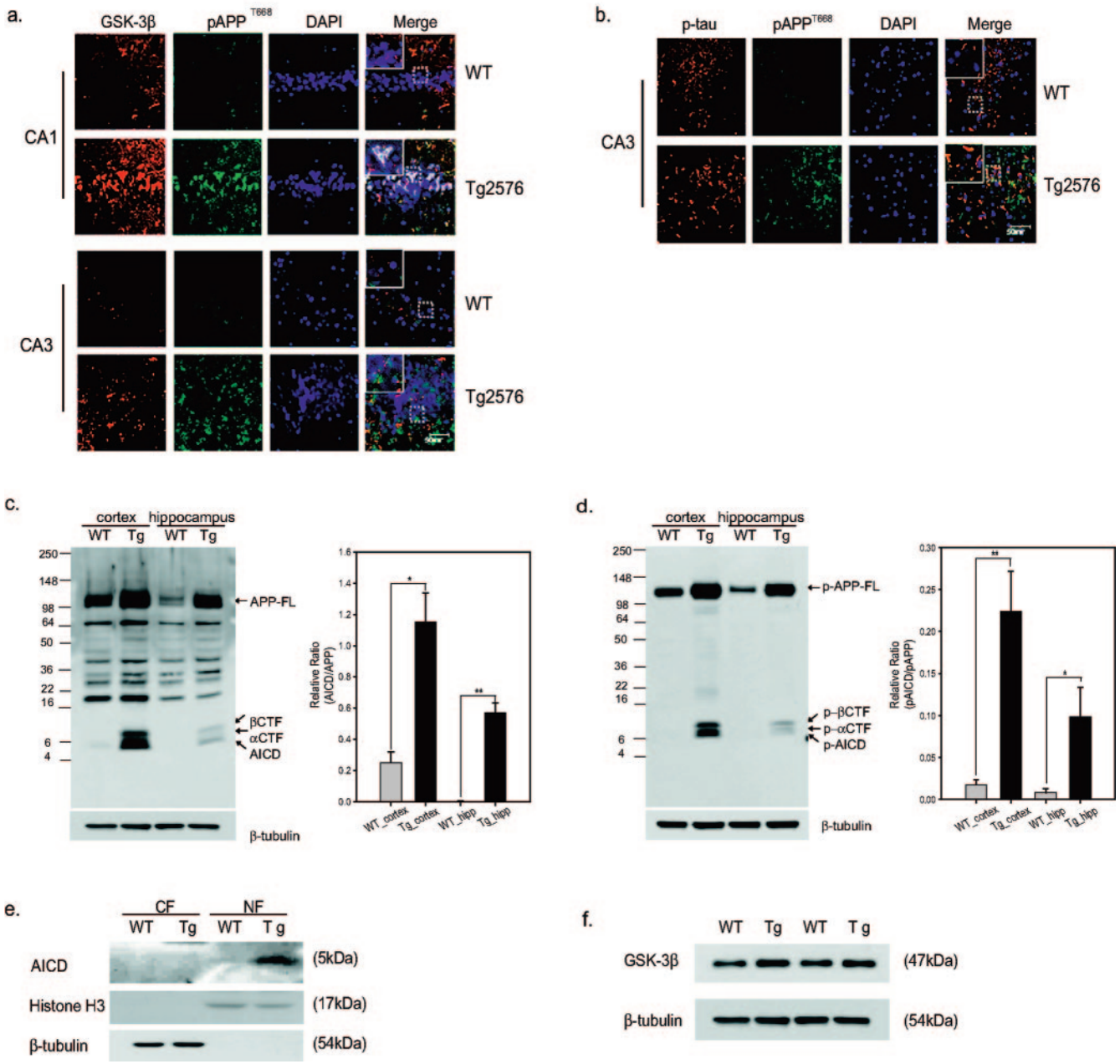

FIG. 7. pAPP^{T668}, GSK-3β, and p-tau are upregulated in Tg2576 mouse brains. The Tg2576 mouse brains ($n = 5$) fixed in 10% neutral buffered formalin for 48 h were dehydrated and embedded in paraffin. The fluorescent immunohistochemistry was performed with appropriate primary antibodies for 2 h and visualized using Cy3-conjugated or fluorescein isothiocyanate-conjugated secondary antibody (Jackson, West Grove, Pennsylvania). DAPI counterstaining was performed. Images were collected using the LSM 510 program on a Zeiss confocal microscope. (a) The immunoreactivities of pAPP^{T668} (green) and GSK-3β (red) were examined in CA1 and CA3 of Tg2576 mouse brains (Tg2576) and WT mouse brains. DAPI staining shows the location of the nucleus (blue). Bar, 50 μm. Magnification, ×353.44. (b) Immunoreactivities of pAPP^{T668} (green) and p-tau (red) were examined in Tg2576 mice and WT mouse brains. Bar, 50 μm. Magnification, ×353.44. (c, d) Protein levels of AICD and CTFs were examined by immunoblotting using C9 antibody which recognizes the last 9 amino acids of APP (c) and anti-pAPP (T668) antibody (d) in the total lysates of cortex or hippocampus in Tg2576 mice and WT mouse brains. Densitometric analysis was done, and data represent the means ± standard errors of results from three or six separate experiments. **, $P < 0.01$; *, $P < 0.05$ (by ANOVA). (e) The presence of the AICD was checked in nuclear fraction (NF) and the cytoplasmic fraction (CF) from the cortices in Tg2576 mouse brains by immunoblotting using C9 antibody. (f) Protein levels of GSK-3β were examined in cortex in WT and Tg2576 mouse brains by immunoblotting using anti-GSK-3β antibody.

We found that GSK-3β promoter activity was significantly increased by 3 to 4-fold in the cells after cotransfection of human GSK-3β promoter in the PGL2 vector, Fe65, and AICD construct. Human GSK-3β promoter has several potential transcriptional factor binding sites including two CP2 binding sites. Putative CP2 binding sites are present at nt −1292 to −1282 and nt −1 to +10 (20). Using the deletion mutants without nt −1292 to −1282 (GCGCACACCAA) or nt −1 to

+10 (GCCCGGGCCAA), we performed a luciferase activity assay following cotransfection of the AICD with one of these deletion mutants of the human GSK-3β promoter in the pGL2 luciferase vector. Deletions of the CP2 binding site inhibit the increase of the promoter activity by the AICD. By contrast, the inhibition of phosphorylation by the T668A point mutation significantly reduced the increase in the human GSK-3β promoter activity. By this result, we can infer that the binding of the ternary complex of phosphorylated AICD, Fe65, and CP2 to CP2 binding sites in the GSK-3β promoter region initiates the gene transcription of GSK-3β.

It was reported that strong immunoreactivities against the phosphorylated form of GSK-3β were observed in a subpopulation of neurons with neurofibrillary tangles and were also observed in dystrophic neurites of senile plaques, neuropil threads, Pick bodies, tau-containing astrocytes, and coiled bodies (10). Also, both in transfected cells (22) and in vivo (12, 23), GSK-3β has been known to phosphorylate tau in most hyperphosphorylated sites in PHFs. One of the hallmarks, neurofibrillary tangles, of AD is formed by insoluble intracellular polymers of hyperphosphorylated tau, the less-phosphorylated forms of which stabilize the microtubules of the axonal cytoskeleton (36). Hyperphosphorylated tau is considered one of the earliest signs of neuronal degeneration.

We also examined whether the phosphorylation of C50 at T668 induced tau phosphorylation at the Ser^{202} and Thr^{205} residues. The hyperphosphorylated form of tau is the major component of the PHFs and neurofibrillary tangles and is believed to cause apoptosis by disrupting cytoskeletal and axonal transport. We found a significant increase in tau phosphorylated at Ser^{202} and Thr^{205} in C50-transfected cells, but no increase was observed in the deletion mutant or in T668A mutant-transfected cells. This finding suggests that the phosphorylation of AICD at T668 is critically required for its nuclear translocation and for GSK-3β induction, followed by tau phosphorylation.

We also show that inhibition of T668 phosphorylation of AICD by inhibitors or mutations of T668 sites dramatically reduced its translocation to the nucleus and the resultant neurotoxicity. We confirmed that treatment with 40 μM olomoucine (a cdc2 kinase inhibitor), 5 μM roscovitine (a cdk5 inhibitor), or 10 mM LiCl (a GSK-3β inhibitor) for 48 h significantly reduced the phosphorylated form of C50 at T668, GSK-3β expression, tau phosphorylation induced by C50, and GSK-3β promoter activity induced by C50. Decreased cell viability by C50 was overcome by treating each of the three kinase inhibitors, indicating that the phosphorylation of C50 at T668 is critical for inducing GSK-3β expression, which leads to increased tau phosphorylation and neurotoxicity.

These results led us to conclude that phosphorylation of AICD at T668 is required for exerting neurotoxicity via transcription-dependent mechanisms by forming an AICD-Fe65-CP2 complex in the nucleus and inducing GSK-3β gene expression, followed by tau phosphorylation. We found that cells expressing the AICD showed significant staining with TUNEL and dysmorphic nuclei compared to the mock-transfected group, whereas deletion mutants (dC50) or T668A mutants ($C50^{T668A}$) displayed fewer apoptotic nuclei than those transfected with C50, suggesting that apoptotic cell death induced by the AICD is related to the YENPTY domain as well as to phosphorylation at T668. Therefore, our results suggest that specific inhibition for APP phosphorylation at T668 could be an important target for AD therapy.

In addition, we also provide in vivo evidence that phosphorylated APP-CTFs at T668, GSK-3β, and p-tau are significantly upregulated in the serial brain sections of the human AD brains and Tg2576 mouse brains. The cytoplasmic and nuclear immunoreactivities of p-APP^{T668} were observed in AD brain tissues and in the Tg2576 mouse brains. More intense staining of p-APP^{T668} was observed in hippocampal pyramidal neurons and in neurons of the dentate gyrus and of the ectorhinal cortex in AD brains and Tg2576 mouse brains than in those of age-matched controls. Tg2576 mouse is an AD animal model which overexpresses Swedish APP, a familial APP mutant gene. To compare the levels of p-APP-CTFs in Tg 2576 mice versus WT mice, we normalized total AICD versus total APP. The ratios of phosphorylated AICD at T668 versus total APP were significantly higher in Tg2576 mice than in WT mice (Fig. 7c, d). These results strongly suggest that T668 phosphorylation might be a contributing factor to AD pathology in this AD. Intense GSK-3β immunoreactivity and tau phosphorylation were also detected in the cytoplasm of hippocampal and ectorhinal cortical neurons in AD brains (Braaks stage V) (6) and in Tg2576 mouse brains. Additionally, increased neuronal death was observed in the serial sections of hippocampal regions showing p-APP^{T668} immunoreactivities. These findings strongly suggest that an increase in p-APP^{T668} may be closely related to the pathogenesis of cell death in AD via regulation of GSK-3β and p-tau.

Taken together, these results suggest that phosphorylation of the AICD at T668 contributes to the neuronal degeneration in AD by regulating its translocation into the nucleus and then inducing neurodegeneration and that the specific inhibitor of T668 phosphorylation might be the target of AD therapy.

ACKNOWLEDGMENTS

We are grateful to S. H. Kim and S. S. Sisodia at the University of Chicago for providing APP695 cDNA. We also thank P. C. Shaw for providing human GSK-3β promoter in pCAT vector and T. Sudhof for APP-Gal4 and AICD-Gal4 constructs.

This work was financially supported by a National Creative Research Initiative Grant (2003–2005) from MOST and in part by the BK21 Human Life Sciences project.

REFERENCES

1. **Ando, K., K. I. Iijima, J. I. Elliott, Y. Kirino, and T. Suzuki.** 2001. Phosphorylation-dependent regulation of the interaction of amyloid precursor protein with Fe65 affects the production of beta-amyloid. J. Biol. Chem. **276:**40353–40361.
2. **Ando, K., M. Oishi, S. Takeda, K. Iijima, T. Isohara, A. C. Nairn, Y. Kirino, P. Greengard, and T. Suzuki.** 1999. Role of phosphorylation of Alzheimer's amyloid precursor protein during neuronal differentiation. J. Neurosci. **19:**4421–4427.
3. **Aplin, A. E., G. M. Gibb, J. S. Jacobsen, J. M. Gallo, and B. H. Anderton.** 1996. In vitro phosphorylation of the cytoplasmic domain of the amyloid precursor protein by glycogen synthase kinase-3beta. J. Neurochem. **67:**699–707.
4. **Baek, S. H., K. A. Ohgi, D. W. Rose, E. H. Koo, C. K. Glass, and M. G. Rosenfeld.** 2002. Exchange of N-CoR corepressor and Tip60 coactivator complexes links gene expression by NF-κB and β-amyloid precursor protein. Cell **110:**55–67.
5. **Borg, J. P., J. Ooi, E. Levy, and B. Margolis.** 1996. The phosphotyrosine interaction domains of X11 and Fe65 bind to distinct sites on the YENPTY motif of amyloid precursor protein. Mol. Cell. Biol. **16:**6229–6241.
6. **Braak, H., and E. Braak.** 1991. Neuropathological stageing of Alzheimer-related changes. Acta Neuropathol. (Berlin) **82:**239–259.
7. **Buxbaum, J. D., G. Thinakaran, V. Koliatsos, J. O'Callahan, H. H. Slunt,**

D. L. Price, and S. S. Sisodia. 1998. Alzheimer amyloid protein precursor in the rat hippocampus: transport and processing through the perforant path. J. Neurosci. **18:**9629–9637.
8. **Cao, X., and T. C. Südhof.** 2001. A transcriptionally [correction of transcriptively] active complex of APP with Fe65 and histone acetyltransferase Tip60. Science **293:**115–120.
9. **Duilio, A., R. Faraonio, G. Minopoli, N. Zambrano, and T. Russo.** 1998. Fe65L2: a new member of the Fe65 protein family interacting with the intracellular domain of the Alzheimer's beta-amyloid precursor protein. Biochem. J. **330**(Pt 1)**:**513–519.
10. **Ferrer, I., M. Barrachina, and B. Puig.** 2002. Glycogen synthase kinase-3 is associated with neuronal and glial hyperphosphorylated tau deposits in Alzheimer's disease, Pick's disease, progressive supranuclear palsy and corticobasal degeneration. Acta Neuropathol. (Berlin) **104:**583–591.
11. **Fiore, F., N. Zambrano, G. Nimopoli, V. Dnini, A. Duilio, and T. Russo.** 1995. The regions of Fe65 protein homologous to the phosphotyrosine interaction/phosphotyrosine binding domain of the Shc bind the intracellular domain of the Alzheimer's amyloid precursor protein. J. Biol. Chem. **270:** 30853–30856.
12. **Hong, M., D. C. Chen, P. S. Klein, and V. M. Lee.** 1997. Lithium reduces tau phosphorylation by inhibition of glycogen synthase kinase-3. J. Biol. Chem. **272:**25326–25332.
13. **Hsiao, K., P. Chapman, S. Nilsen, C. Eckman, Y. Harigaya, S. Younkin, F. Yang, and G. Cole.** 1996. Correlative memory deficits, Abeta elevation, and amyloid plaques in transgenic mice. Science **274:**99–102.
14. **Iijima, K., K. Ando, S. Takeda, Y. Satoh, T. Seki, S. Itohara, P. Greengard, Y. Kirino, A. C. Nairn, and T. Suzuki.** 2000. Neuron-specific phosphorylation of Alzheimer's beta-amyloid precursor protein by cyclin-dependent kinase 5. J. Neurochem. **75:**1085–1091.
15. **Kim, H. S., E. M. Kim, J. P. Lee, C. H. Park, S. Kim, J. H. Seo, K.-A. Chang, E. Yu, S. J. Jeong, Y. H. Chong, et al.** 2003. C-terminal fragments of amyloid precursor protein exert neurotoxicity by inducing glycogen synthase kinase-3beta expression. FASEB J. **17:**1951–1953.
16. **Kimberly, W. T., J. B. Zheng, S. Y. Guenette, and D. J. Selkoe.** 2001. The intracellular domain of the beta-amyloid precursor protein is stabilized by Fe65 and translocates to the nucleus in a notch-like manner. J. Biol. Chem. **276:**40288–40292.
17. **Kimberly, W. T., J. B. Zheng, T. Town, R. A. Flavell, and D. J. Selkoe.** 2005. Physiological regulation of the beta-amyloid precursor protein signaling domain by c-Jun N-terminal kinase JNK3 during neuronal differentiation. J. Neurosci. **25:**5533–5543.
18. **Kinoshita, A., C. M. Whelan, C. J. Smith, O. Berezovska, and B. T. Hyman.** 2002. Direct visualization of the gamma secretase-generated carboxyl-terminal domain of the amyloid precursor protein: association with Fe65 and translocation to the nucleus. J. Neurochem. **82:**839–847.
19. **Koo, J. W., C. H. Park, S. H. Choi, N. J. Kim, H. S. Kim, J. C. Choe, and Y. H. Suh.** 2003. The postnatal environment can counteract prenatal effects on cognitive ability, cell proliferation, and synaptic protein expression. FASEB J. **217:**1556–1558.
20. **Lau, K. F., C. C. J. Miller, B. H. Anderton, and P. C. Shaw.** 1999. Molecular cloning and characterization of the human glycogen synthase kinase-3β promoter. Genomics **60:**121–128.
21. **Lee, M. S., S. C. Kao, C. A. Lemere, W. Xia, H. C. Tseng, Y. Zhou, R. Neve, M. K. Ahlijanian, and L. H. Tsai.** 2003. APP processing is regulated by cytoplasmic phosphorylation. J. Cell Biol. **163:**83–95.
22. **Lovestone, S., C. H. Reynolds, D. Latimer, D. R. Davis, B. H. Anderton, J. M. Gallo, D. Hanger, S. Mulot, B. Marquardt, S. Stabel, et al.** 1994. Alzheimer's disease-like phosphorylation of the microtubule-associated protein tau by glycogen synthase kinase-3 in transfected mammalian cells. Curr. Biol. **4:**1077–1086.
23. **Munoz-Montano, J. R., F. J. Moreno, J. Avila, and J. Diaz-Nido.** 1997. Lithium inhibits Alzheimer's disease-like tau protein phosphorylation in neurons. FEBS Lett. **411:**183–188.
24. **Pardossi-Piquard, R., A. Petit, T. Kawarai, C. Sunyach, C. Alves da Costa, B. Vincent, S. Ring, L. D'Adamio, J. Shen, U. Muller, P. St. George Hyslop, and F. Checler.** 2005. Presenilin-dependent transcriptional control of the Aβ-degrading enzyme neprilysin by intracellular domains of βAPP AND APLP. Neuron **46:**541–554.
25. **Ramelot, T. A., and L. K. Nicholson.** 2001. Phosphorylation-induced structural changes in the amyloid precursor protein cytoplasmic tail detected by NMR. J. Mol. Biol. **307(3):**871–884.
26. **Russo, T., R. Faraonio, G. Minopoli, P. De Candia, S. De Renzis, and N. Zambrano.** 1998. Fe65 and the protein network centered around the cytosolic domain of the Alzheimer's beta-amyloid precursor protein. FEBS Lett. **434:**1–7.
27. **Sastre, M., R. S. Turner, and E. Levy.** 1998. X11 interaction with beta-amyloid precursor protein modulates its cellular stabilization and reduces amyloid beta-protein secretion. J. Biol. Chem. **273:**22351–22357.
28. **Selkoe, D. J.** 1991. The molecular pathology of Alzheimer's disease. Neuron **6:**487–498.
29. **Selkoe, D. J.** 2001. Alzheimer's disease: genes, proteins, and therapy. Physiol. Rev. **81:**741–766.
30. **Standen, C. L., J. Brownlees, A. J. Grierson, S. Kesavapany, K. F. Lau, D. M. McLoughlin, and C. C. Miller.** 2001. Phosphorylation of thr(668) in the cytoplasmic domain of the Alzheimer's disease amyloid precursor protein by stress-activated protein kinase 1b (Jun N-terminal kinase-3). J. Neurochem. **76:**316–320.
31. **Suh, Y. H., and F. Checler.** 2002. Amyloid precursor protein, presenilins, and alpha-synuclein: molecular pathogenesis and pharmacological applications in Alzheimer's disease. Pharmacol. Rev. **54:**469–525.
32. **Suzuki, N., T. T. Cheung, X. D. Cai, A. Odaka, L. Otvos, C. Eckman, Jr., T. E. Golde, and S. G. Younkin.** 1994. An increased percentage of long amyloid beta protein secreted by familial amyloid beta protein precursor (beta APP717) mutants. Science **264:**1336–1340.
33. **Taru, H., K. Iijima, M. Hase, Y. Kirino, Y. Yagi, and T. Suzuki.** 2002. Interaction of Alzheimer's β-amyloid precursor family proteins with scaffold proteins of the JNK signaling cascade. J. Biol. Chem. **277:**20070–20078.
34. **Taru, H., and T. Suzuki.** 2004. Facilitation of stress-induced phosphorylation of beta-amyloid precursor protein family members by X11-like/Mint2 protein. J. Biol. Chem. **279:**21628–21636.
35. **Telese, F., P. Bruni, A. Donizetti, D. Gianni, C. D'Ambrosio, A. Scaloni, N. Zambrano, M. G. Rosenfeld, and T. Russo.** 2005. Transcription regulation by the adaptor protein Fe65 and the nucleosome assembly factor SET. EMBO Rep. **6:**77–82.
36. **Trojanowski, J. Q., M. L. Schmidt, R. W. Shin, G. T. Bramblett, M. Goedert, and V. M. Y. Lee.** 1993. From pathological marker to potential mediator of neuronal dysfunction and degeneration in Alzheimer's disease. Clin. Neurosci. **1:**184–191.
37. **Vassar, R., and M. Citron.** 2000. Abeta-generating enzymes: recent advances in beta- and gamma-secretase research. Neuron **27:**419–422.
38. **Von Rotz, R. C., B. M. Kohli, J. Bosset, M. Meier, T. Suzuki, R. M. Nitsch, and U. Konietzko.** 2004. The APP intracellular domain forms nuclear multiprotein complexes and regulates the transcription of its own precursor. J. Cell Sci. **117:**4435–4448.
39. **Wolfe, M. S., and C. Haass.** 2001. The role of presenilins in gamma-secretase activity. J. Biol. Chem. **276:**5413–5416.
40. **Zambrano, N., P. Bruni, G. Minopoli, R. Mosca, D. Molino, C. Russo, G. Schettini, M. Sudol, and T. Russo.** 2001. The beta-amyloid precursor protein APP is tyrosine-phosphorylated in cells expressing a constitutively active form of the Abl protoncogene. J. Biol. Chem. **276:**19787–19792.
41. **Zambrano, N., G. Minopoli, P. de Candia, and T. Russo.** 1998. The Fe65 adaptor protein interacts through its PID1 domain with the transcription factor CP2/LSF/LBP1. J. Biol. Chem. **273:**20128–20133.
42. **Zheng, P., J. Eastman, P. S. Vande, and S. W. Pimplikar.** 1998. PAT1, a microtubule-interacting protein, recognizes the basolateral sorting signal of amyloid precursor protein. Proc. Natl. Acad. Sci. USA **95:**14745–14750.